Computational problems in magnetic resonance imaging

Tuomo Valkonen, University of Cambridge

Joint work with M. Benning, L. Gladden, D. Holland, C.-B. Schönlieb (Cambridge), K. Bredies, M. Liebmann (Uni-Graz), and F. Knoll (TU Graz).

Diffusion tensor imaging [7, 8]

- Diffusion-weighted MRI measures diffusion of water molecules along gradient b_i.
- The DWI images s_i are connected by the Stejskal-Tanner equation
$$s_i(x) = s_0(x)\exp(-\langle b_i \otimes b_i, u(x)\rangle) \qquad (1)$$
to a *diffusion tensor field* u, describing a pointwise Gaussian PDF.
- Applications include discovery of neural pathways by tractography on u, useful for detecting pathologies.

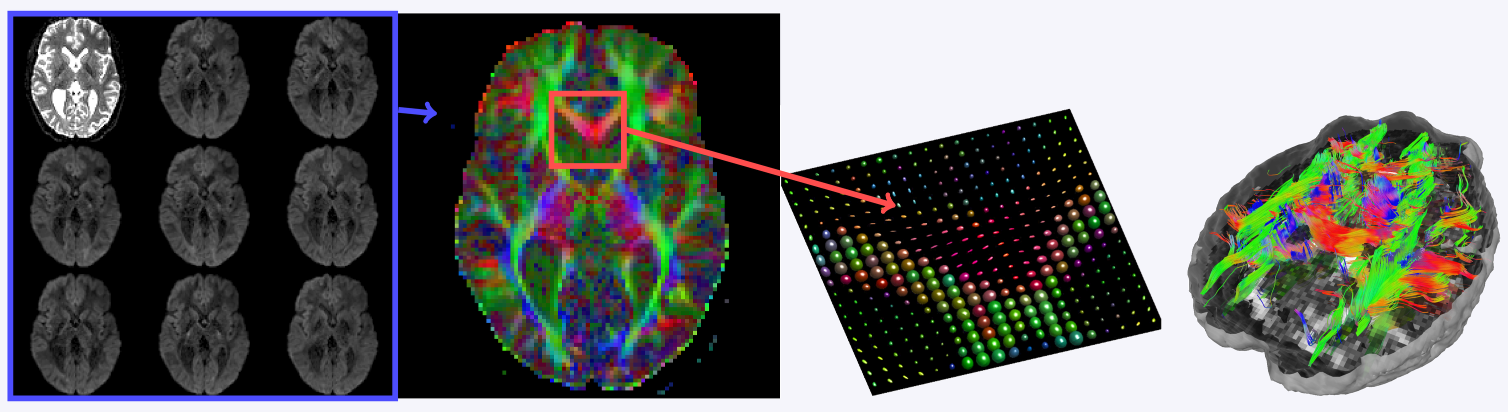

Figure: Illustration of the DTI process. Left-to-right: 1. DWI images, 2. colour-coded tensors, 3. zoom into corpus callosum, 4. tractography.

Denoising DTI volumes

- The DWI process is inherently noisy. We therefore seek to denoise u using a variational regularisation approach.
- Options include **(A)** reconstruct u first from (1), then denoise, and **(B)** reconstruct simultaneously, incorporating log of (1) into the fidelity term.
- Both options yield for some $(\mathcal{A}u)(x) = A(u(x))$ and f problems of the form
$$\min_{u\geq 0} \frac{1}{2}\|f - \mathcal{A}u\|_2^2 + R(u), \qquad (2)$$
with R the regulariser. We stress the pointwise positivity contraint. Non-positive diffusions tensors are non-physical.

Second-order Total Generalised Variation (TGV^2)

- Regularisation by TGV^2 [1] avoids the stair-casing effect of Total Variation (TV), while preserving edges – important on white/grey matter boundary.
- Can be formulated as the differentiation cascade [2]
$$\mathrm{TGV}^2_{(\beta,\alpha)}(u) := \min_w \alpha\|Du - w\|_{\mathcal{M}(\Omega;\mathbb{R}^m)} + \beta\|Ew\|_{\mathcal{M}(\Omega;\mathbb{R}^{m\times m})}.$$
Here Ew is the symmetrised differential, roughly $(Dw + Dw^T)/2$.
- Balances between first and second-order features through w.

Big data, small problems

- We apply the Chambolle-Pock (PDHGM) method [3] to (2).
- In doing so, we have to calculate the resolvent $(I + \tau\partial G)^{-1}(v)$ of $G(u) := \|f - \mathcal{A}u\|_2^2/2$. This involves solving pointwise $u(x)$ from
$$(I + \tau A^*A)u(x) + N_{\geq 0}(v(x)) \ni v(x) + \tau A^* f(x).$$
- **Potentially millions of small but expensive parallel problems**.
  - Typical low-resolution DTI volume in the range $128\times 128\times 64 \approx 1$ megavoxels.
  - In approach **(A)**, $\mathcal{A} = I$, so a projection to the positive definite cone with the QR algorithm.
  - In approach **(B)**, $\mathcal{A} \neq I$, but interior point methods for quadratic SDP [6] applicable.
  - Also possible to reformulate **(B)** as $\|f - \mathcal{A}u\|^2/2 = \sup_\lambda\langle\lambda, f - \mathcal{A}u\rangle - \|\lambda\|^2/2$ and use QR. PDHGM converges slower for this formulation, but can be faster in practise; see [8].

Results, including GPU performance

Table: Computations on a 128×128 slice. Parameter α with smallest Frobenius 2-norm error; $\beta = \alpha$. Decrease of pseudo-duality gap to 0.1% from zero initialisation. [8]

Model	α	Error	Its.
Noisy data		0.03195	
(A), unconstr.	0.00030	0.02480	69
(B), unconstr.	0.00024	0.02554	58
(A), constr.	0.00024	0.02183	63
(B), constr.	0.00018	0.02159	51

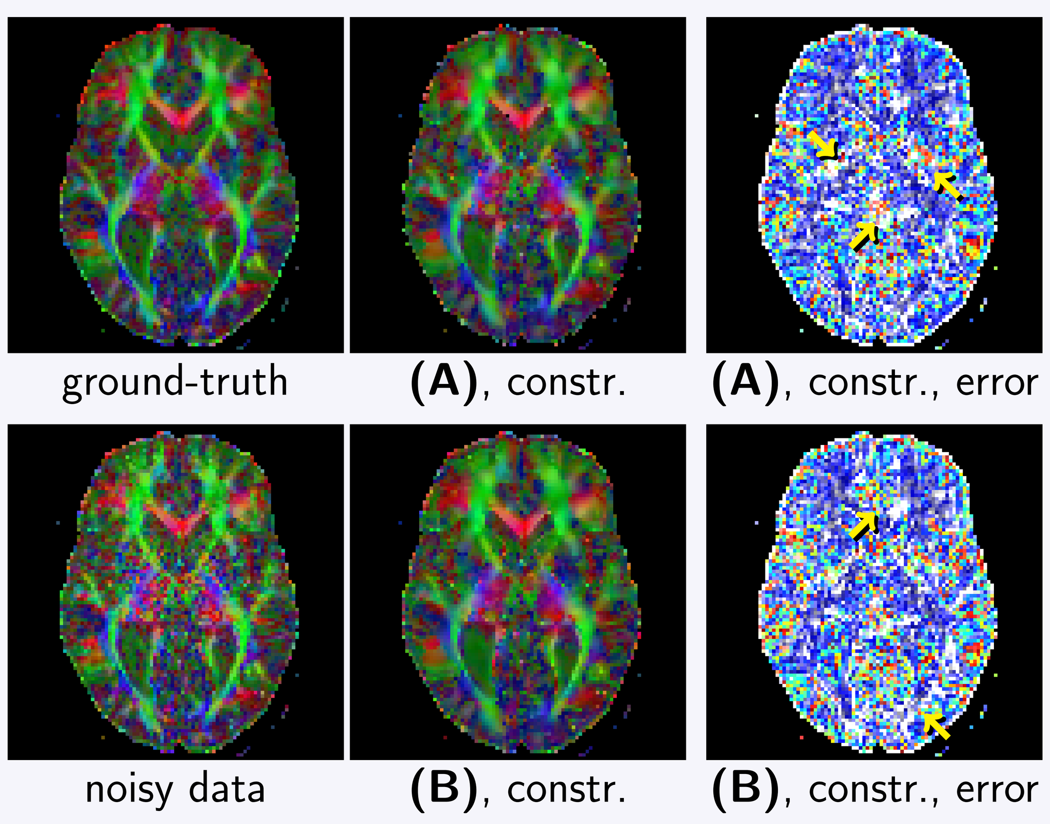

Colour-codings of 1. the principal eigenvector, and 2. errors in its direction and fractional anisotropy.

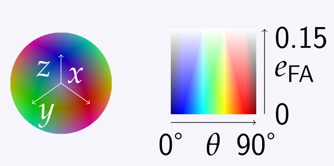

Figure: Visualisation of results. Arrows indicate areas where an approach performs clearly worse than the other.

Table: GPU performance advantage over 1×CPU core (of Intel Xeon X5650) full 3D data ($128\times 128\times 60$), approach **(A)**. Left: advantage, right: computational times. [9]

Hardware	double precision	single precision
GeForce GTX 480	~64×	~108×
Tesla C2070	~45×	~72×

Hardware	One iteration (double prec.)	Full run (1178 its.)
1× CPU core	9s	3h
1× Tesla	0.2s	3m50s

MRI phase reconstruction for velocity imaging

- We are given sub-sampled k-space measurements f. Task: find a "good-quality" image u with $\|f - S\mathcal{F}u\|_2^2$ small. Here S denotes a sub-sampling operator and $\mathcal{F}$ the Fourier transform.
- We are mostly interested in the phase ϕ of $u = \rho\exp(i\phi)$: The phase difference $\phi_1 - \phi_2$ of images u_1 and u_2 is related to the velocity of a fluid.
- Incorporating a-priori information in terms of a regulariser R, we solve
$$\min_u \|f - S\mathcal{F}u\|_2^2 + \alpha R(u).$$

Compare [4] for a wavelet approach. Here we concentrate on TV and TGV^2.

Bregman iteration

- The above minimisation scheme suffers from loss of contrast.
- For homogeneous R this can be compensated by considering [5]
$$u_k \in \arg\min_u \left\{\|f - S\mathcal{F}u\|_2^2 + \alpha D_R^{p_{k-1}}(u, u_{k-1})\right\}$$
with
$$D_R^{p_{k-1}}(u, u_{k-1}) = R(u) - R(u_{k-1}) - \langle p_{k-1}, u - u_{k-1}\rangle.$$
- **Computationally challenging**, inner (PDHGM) + outer iterations.
- We use the discrepancy principle
$$\|f - S\mathcal{F}u_k\|_2 \leq \delta$$
to stop the Bregman iterations, knowing noise level δ. Its applicability is verified in the Figure, comparing against optimal PSNR.

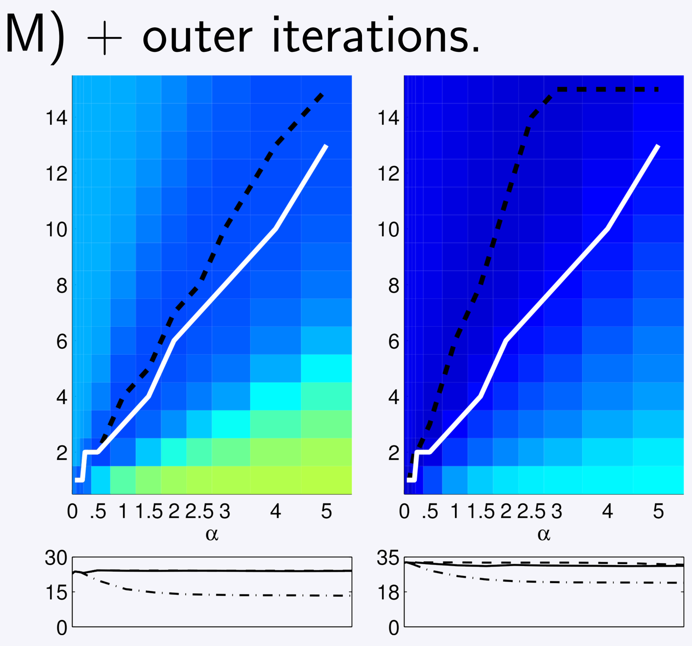

(a) Amplitude ρ (b) Phase ϕ

Figure: PSNR plot for $R = $ TV, varying α and Bregman iteration. Solid line: discrepancy principle, dashed line: optimal PSNR, dash-dotted line: first iteration.

Computational results

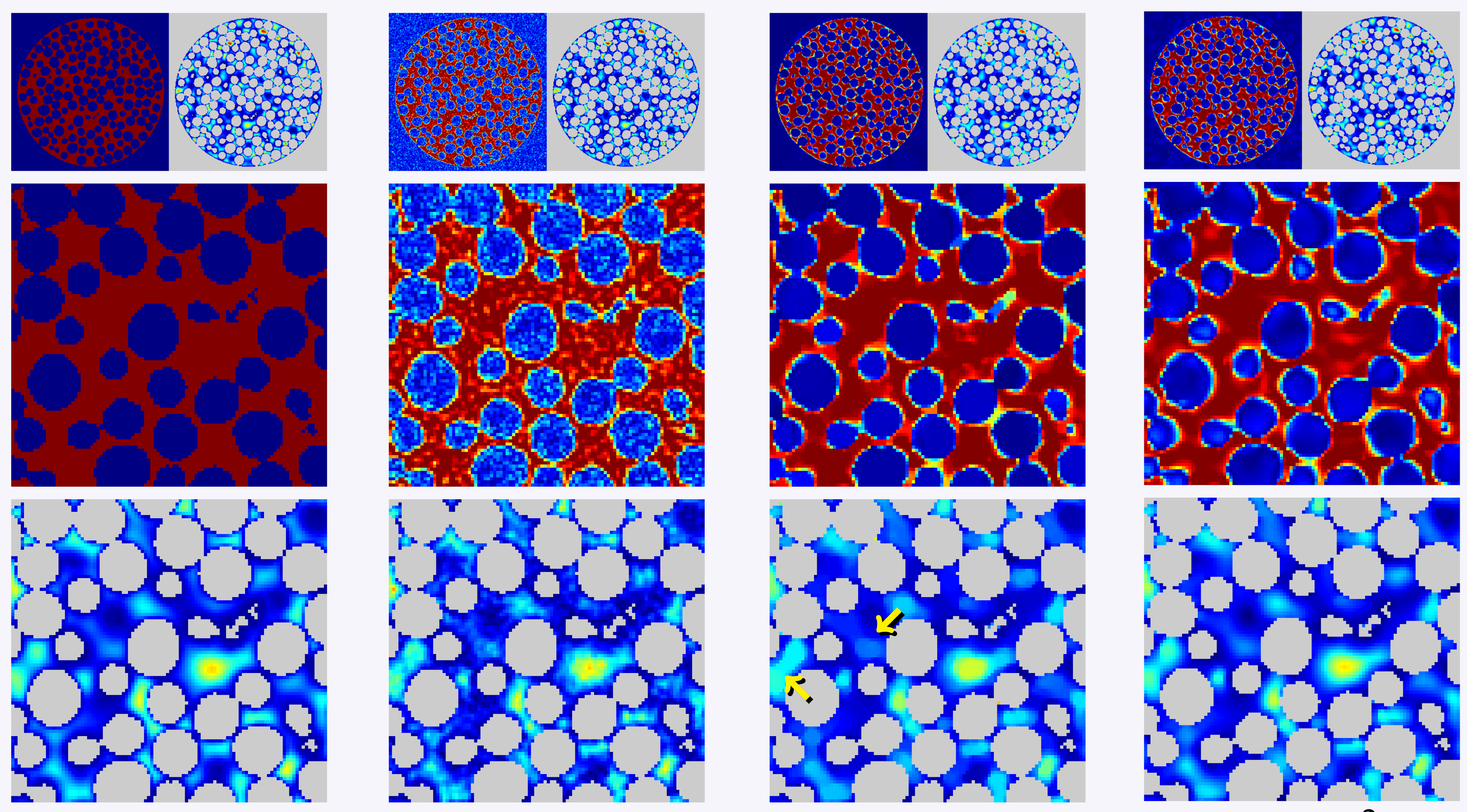

(c) Ground-truth (d) Noise+subspl. (e) TV (f) TGV^2

Figure: Bregmanised TV and TGV^2 reconstruction from noisy sub-sampled data at violation of the discrepancy principle. Arrows indicate the stair-casing of TV, avoided by TGV^2.

References

[1] K. Bredies, K. Kunisch and T. Pock, *Total generalized variation*, SIAM J. Imaging Sci. **3** (2011), 492–526.

[2] K. Bredies and T. Valkonen, *Inverse problems with second-order total generalized variation constraints*, in: *Proceedings of SampTA 2011*, Singapore, 2011.

[3] A. Chambolle and T. Pock, *A first-order primal-dual algorithm for convex problems with applications to imaging*, J. Math. Imaging Vision **40** (2011), 120–145.

[4] D. Holland, D. Malioutov, A. Blake, A. Sederman and L. Gladden, *Reducing data acquisition times in phase-encoded velocity imaging using compressed sensing*, Journal of Magnetic Resonance **203** (2010), 236–246.

[5] S. Osher, M. Burger, D. Goldfarb, J. Xu and W. Yin, *An iterative regularization method for total variation-based image restoration*, SIAM Multiscale Model. Simul. **4** (2005), 460–489.

[6] T. Valkonen, *A method for weighted projections to the positive definite cone*, SFB-Report 2012-016, Karl-Franzens University of Graz (2012).

[7] T. Valkonen, K. Bredies and F. Knoll, *Total generalised variation in diffusion tensor imaging*, SIAM J. Imaging Sci. **6** (2013), 487–525.

[8] T. Valkonen, F. Knoll and K. Bredies, *TGV for diffusion tensors: A comparison of fidelity functions*, in: *Journal of Inverse and Ill-posed problems special issue for IP:M&S 2012*, Antalya, Turkey, 2012. Published online.

[9] T. Valkonen and M. Liebmann, *GPU-accelerated regularisation of large diffusion-tensor volumes*, in: *Computing special issue for ESCO 2012*, Pilsen, Czech Republic, 2012. To appear.

Acknowledgements

This work has been supported by King Abdullah University of Science and Technology (KAUST) Award No. KUK-I1-007-43, EPSRC / Isaac Newton Trust Small Grant "Non-smooth geometric reconstruction for high resolution MRI imaging of fluid transport in bed reactors", and Austrian Science Fund (FWF) grant SFB F32 "Mathematical Optimization in Biomedical Sciences".